Unfolding of the [Cu-2(1,3-bis(9-methyl-1,10-phenanthrolin-2-yl)propane)(2)](2+) Helicate. Coupling of the Chlorocarbon Dehalogenation to the Unfolding Process

ARTICLE *in* INORGANIC CHEMISTRY · MARCH 2010

Impact Factor: 4.76 · DOI: 10.1021/ic9018986 · Source: PubMed

8 AUTHORS, INCLUDING:

G. Ferraudi
University of Notre Dame
186 PUBLICATIONS **2,506** CITATIONS
SEE PROFILE

Aleaander Graham Lappin
University of Notre Dame
93 PUBLICATIONS **1,464** CITATIONS
SEE PROFILE

Allen G Oliver
University of Notre Dame
185 PUBLICATIONS **2,318** CITATIONS
SEE PROFILE

Bruce C Noll
Bruker AXS Inc.
286 PUBLICATIONS **6,693** CITATIONS
SEE PROFILE

Inorganic Chemistry
Article

Inorg. Chem. **2010**, *49*, 4023–4035 **4023**
DOI: 10.1021/ic9018986

Unfolding of the $[Cu_2(1,3\text{-bis}(9\text{-methyl-}1,10\text{-phenanthrolin-}2\text{-yl})\text{propane})_2]^{2+}$ Helicate. Coupling of the Chlorocarbon Dehalogenation to the Unfolding Process

L. Lemus,[†] J. Guerrero,[†] J. Costamagna,[†] G. Estiu,*[,‡] G. Ferraudi,*[,§] A. Graham Lappin,*[,‡] A. Oliver,[‡] and B. C. Noll[‡]

[†]*Facultad de Química y Biología, Universidad de Santiago de Chile, Av. Libertador Bernardo ÓHiggins 3363, Estación Central, Santiago, Chile,* [‡]*Department of Chemistry and Biochemistry, and* [§]*Radiation Research Building, University of Notre Dame, Notre Dame, Indiana 46556*

Received September 25, 2009

A new helical dimeric copper(I) complex $[Cu_2(mphenpr)_2](ClO_4)_2$ where mphenpr is 1,3-bis(9-methyl-1,10-phenanthrolin-2-yl)propane has been prepared and characterized by X-ray crystallography and NMR. In the solid state, the metal centers are 6.42 Å apart, and the electronic structure has been investigated with use of density functional theory (DFT) calculations. In solution the dimer equilibrates with a monomeric form $[Cu(mphenpr)](ClO_4)$, and the mechanism of unfolding of the dimer into monomer has been studied. In the presence of CCl_4, formation of the monomer is coupled to the reductive dehalogenation of the halocarbon. The mechanism of this process has been probed by the study of short-lived potential reaction intermediates using fast kinetic pulse radiolysis techniques and comparisons with DFT calculations. The copper(II) product $[Cu(mphenpr)Cl](ClO_4)$ and an analogue $[Cu(mphenpr)](ClO_4)_2$ have been isolated and characterized by X-ray crystallography.

Introduction

Numerous examples of supramolecular assemblies based on selective metal to ligand interactions have been engineered during the past few years.[1−3] Many of them rely on the coordination of transition metal cations to polypyridine and phenanthroline fragments incorporated into oligomeric ribbons or macroscopic loops.[4] These ligands contain multiple metal binding sites with donor sets that match the coordination geometry requirements of specific metals, giving rise to multistranded helical arrays.[3,5−8] In particular, copper(I) helicate complexes have been used as a platform to develop much fundamental supramolecular chemistry.[8,9] The tetrahedral coordination of copper(I) defines the orientation of the ligand strands that directs the coordination of additional copper ions into the spontaneous formation of chiral double helices.

Helicate assemblies have gained popularity for aesthetic reasons but are nowadays well-known for their applications in diverse areas such as liquid crystals,[10] ion and guest binding[11−13] and DNA recognition.[14−16] The potential applications can be designed by manipulating the structural

*To whom correspondence should be addressed. E-mail: gestiu@nd.edu (G.E.), ferraudi.1@nd.edu (G.F.), lappin.1@nd.edu (A.G.L.).

(1) Saalfrank, R. W.; Maid, H.; Scheurer, A. *Angew. Chem., Int. Ed.* **2008**, *47*, 8794–8824.
(2) Elhabiri, M.; Albrecht-Gary, A. *Coord. Chem. Rev.* **2008**, *252*, 1079–1092 and references therein.
(3) Hannon, M. J.; Childs., L. J. *Supramol. Chem.* **2004**, *16*, 7–22.
(4) Ziessel, R. *Coord. Chem. Rev.* **2001**, *216*, 195–223.
(5) Childs, L. J.; Pascu, M.; Clarke, A. J.; Alcock, N. W.; Hannon., M. J. *Chem.—Eur. J.* **2004**, *10*, 4291–4300.
(6) Reid, S. D.; Blake, A. J.; Wilson, C.; Love, J. B. *Inorg. Chem.* **2006**, *45*, 636–643.
(7) Zhu, A.-X.; Zhang, J.-P.; Lin, Y.-Y.; Chen, X.-M. *Inorg. Chem.* **2008**, *47*, 7389–7395.
(8) Nitschke, J. R.; Schultz, D.; Bernardinelli, G.; Gerard, D. *J. Am. Chem. Soc.* **2004**, *126*, 16538–16543.
(9) (a) Constable, E. C.; Neuburger, M.; Whall, L. A.; Zehnder, M. *New J. Chem.* **1998**, *22*, 219–220. (b) Stefankiewicz, A. R.; Walesa, M.; Jankowski, P.; Ciesielski, A.; Patroniak, V.; Kubicki, M.; Hnatejko, Z.; Harrowfield, J. M.; Lehn, J. M. *Eur. J. Inorg. Chem.* **2008**, 2910–2920. (c) Dietrich-Buchecker, C. O.; Sauvage, J.-P.; Decian, A.; Fischer, J. *J. Chem. Soc., Chem. Commun.* **1994**, 2231–2232. (d) Dietrich-Buchecker, C. O.; Nierengarten, J.-F.; Sauvage, J.-P.; Armaroli, N.; Balzani, V.; De Colalb, L. *J. Am. Chem. Soc.* **1993**, *115*, 11237–11244. (e) Ditrich-Buchecker, C. O.; Nierengarten, J.-F.; Sauvage, J.-P. *Tetrahedron Lett.* **1992**, *33*, 3625–3628. (f) Ditrich-Buchecker, C. O.; Sauvage, J. -P.; Kintzinger, J. P.; Maltese, P.; Pascard, C.; Guilhem, J. *New J. Chem.* **1992**, *16*, 931–942 and references therein.
(10) Douce, L.; Ziessel, R. *Mol. Cryst. Liq. Cryst.* **2001**, *362*, 133–145.
(11) Davis, A. V.; Fiedle, D.; Ziegler, M.; Terpin, A.; Raymond, K. N. *J. Am. Chem. Soc.* **2007**, *129*, 15354–15363.
(12) Goetz, S.; Kruge, P. E. *Dalton Trans.* **2006**, 1277–1284.
(13) Baylies, C. J.; Riis-Johannessen, T.; Harding, L. P.; Jeffery, J. C.; Moon, R.; Rice, C. R.; Whitehead, M. *Angew. Chem., Int. Ed.* **2005**, *44*, 6909–6912.
(14) (a) Malina1, J.; Hannon, M. J.; Brabec, V. *Nucleic Acids Res.* **2008**, *36*, 3630–3638. (b) Peberdy, J. C.; Malina, J.; Khalid, S.; Hannon, M. J.; Rodger, A. *J. Inorg. Biochem.* **2007**, *101*, 1937–1945. (c) Cerasino, L.; Hannon, M. J.; Sletten, E. *Inorg. Chem.* **2007**, *46*, 6245–6251. (d) Oleksi, A.; Blanco, A. G.; Boer, R.; Us, I.; Aymam, J.; Rodger, A.; Hannon, M. J.; Coll, M. *Angew. Chem., Int. Ed.* **2006**, *45*, 1227–1231. (e) McDonnell, U.; Hicks, M. R.; Hannon, M. J.; Rodger, A. *J. Inorg. Biochem.* **2008**, *102*, 2052–2059.
(15) Muller, J.; Lippert, B. *Angew. Chem., Int. Ed.* **2006**, *45*, 2503–2505.
(16) Constable, E. C. *Tetrahedron* **1992**, *48*, 10013–10059.

Published on Web 03/29/2010

characteristics of the complexes. In double or triple helical architectures the design has to contemplate both the nature of the metal and chelating units and the characteristics of the spacer between them.[5,16] The latter has been associated with the preferred stabilization of either a face-to-face or a helicate configuration[17−20] and with the thermodynamic and kinetic stability of boxes and helices.[5,21] Moreover, the spacer can determine whether the two metal binding sites coordinate to one or two metal centers and, in this way, the distance between them.[3,5,22] A large separation between metal units provides the potential to trap small molecules.[22] On the other hand, topological preferences of different oxidation states have been extensively used to build molecular switches and wires.[2,23,24] In this regard, copper(I)/(II) complexes of bidentate ligands have been of particular interest for applications as molecular switches because of the differences in topological preferences between copper(I) and copper(II) cations.[24] Double-helical copper(I) complexes are sensitive to oxidation to form the mixed valence form and/or homovalent copper(II) complexes, which are stabilized as both metal and ligand requirements are satisfied through pentadentate coordination of the copper(II) cation.[25,26]

Our interest in these systems stems from the possibility of discovering reactivity that is dependent on the arrangement of the metals. Early work by Lehn and co-workers[27] and by Yao and co-workers[28] reported the synthesis and investigated redox behavior of bipyridine and phenanthroline copper(I) double-stranded helicates with ethane spacers by electrochemical techniques. In the paper, we report the preparation of a new copper(I) helicate, $[Cu^{I}_2$(1,3-bis(9-methyl-1,10-phenanthrolin-2-yl)propane$)_2]^{2+}$, abbreviated as $[Cu^{I}_2$(mphenpr$)_2]^{2+}$, which is structurally related to the helicate previously reported by Yao et al.,[28] but where the longer spacer increases the separation between the Cu units from 5.73 Å to 6.42 Å

Experimental Section

Materials. Dry tetrahydrofuran (THF) was obtained after refluxing a solution of Na/benzophenone in the commercial THF (Merk) for 24 h under N_2. The dry, peroxide free, THF was then distilled from this solution. Sigma-Aldrich neocuproine (2,9-dimethyl-1,10-phenanthroline), 2,2,6,6-tetrametilpiperidine-1-oxyl (TEMPO), diisopropylamine, butyllithium 1.6 M, diiodomethane, and other solvents besides THF were used as received.

$[Cu(CH_3CN)_4](ClO_4)$ was synthesized following a literature procedure.[29]

1,3-Bis(9-methyl-1,10-phenanthrolin-2-yl)propane (mphenpr). An adaptation of a literature protocol, used for the preparation of dimeric phenanthroline ligands,[30] was followed for the preparation of mphenpr. Freshly prepared lithium diisopropylamide, LDA, was added to a solution of neocuproine (5 g, 24 mmol) in THF until the reaction with the H_2O present in the solution was completed. The absence of the H_2O is noticeable by the blue color of the solution. The temperature of the solution was then lowered to −40 °C under a N_2 atmosphere, and an additional 24 mmol of LDA were added dropwise to the stirred solution. The dark blue liquid was warmed up to −5 °C, kept at this temperature for 1 h, and brought to −20 °C. Diiodomethane (1 mL, 12 mmol) dissolved in THF was added dropwise while stirring the solution, and the resulting mixture was kept at −20 °C for 4 h. To eliminate the excess of LDA, 400 mL of 10% NH_4Cl in H_2O were added after the solution was allowed to warm to room temperature. The reaction products were extracted with 3 × 200 mL of CH_2Cl_2, and the organic phase was rotoevaporated to dryness. The brown solid was dissolved in CH_2Cl_2 and chromatographed on an alumina column to separate the mphenpr from the neocuproine. A 1% (v:v) CH_3OH in CH_2Cl_2 was used as the elutant, and the mphenpr was obtained in a yellow solution. Roto-evaporation of the latter to dryness produced a yellow-brown powder still contaminated with other reaction products. These impurities were eliminated by Soxhlet extraction with ethyl ether. The yield of the pure reaction product was 63%. Anal. Calcd for $C_{29}N_4H_{24}$: H, 5.64; C, 81.28, N, 13.07. Found: H, 5.8; C, 81.0, N, 12.8. The structure of the product as a dimer was assessed by ^{1}H NMR and ^{13}C NMR in CD_3OD. Proton labels are shown in Supporting Information, Figure S1. ^{1}H NMR: δ/ppm 8.22 (d, 2H, J = 8.3 Hz), 8.19 (d, 2H, J = 8.3 Hz), 7.74 (d, 2H, J = 8.8 Hz), 7.71 (d, 2H, J = 8.8 Hz), 7.65 (d, 2H, J = 8.2 Hz), 7.55 (d, 2H, J = 8.2 Hz), 3.29 (t, 4H), 2.83 (s, 6H), 2.50 (q, 2H). ^{13}C NMR: δ/ppm 162.65, 159.03, 144.84, 144.77, 136.67, 127.33, 127.06,125.47, 125.43, 123.26, 123.64, 38.24, 23.60, 30.50.

$[Cu_2$(mphenpr$)_2](ClO_4)_2$. A solution of $[Cu(CH_3CN)_4](ClO_4)$ (3.82 g, 11.7 mmol) in CH_2Cl_2 was added dropwise to a stirred solution of mphenpr (5 g, 11.7 mmol) in CH_2Cl_2. Both solutions were deaerated with streams of N_2, and the mixing of the liquids was conducted under an atmosphere of N_2. The reaction mixture was kept at room temperature for 1 h. Afterward, it was rotoevaporated to dryness to yield the slightly impure $[Cu_2(mphenpr)_2](ClO_4)_2$. This material was washed with $CHCl_3$ and dried under vacuum. Pure $[Cu_2(mphenpr)_2](ClO_4)_2$ precipitated when ethyl ether was slowly diffused into a saturated solution of the complex in CH_3CN. Anal. Calcd for $[Cu_2(C_{29}N_4H_{24})_2](ClO_4)_2$: H, 4.09; C, 58.88, N, 9.47. Found: H, 4.2; C, 59.2, N, 9.2. Mass spectra parent peak m/z = 1083.6 corresponding to $[Cu_2(mphenpr)_2](ClO_4)^+$ (F.W. = 1083.62).

(17) (a) Albrecht-Gary, A. M.; Jansera, I.; Frohlichb, R. *Chem. Commun.* **2005**, 157–165. (b) Meyer, M.; Albrecht-Gary, A. M.; Dietrich-Buchecker, C. O.; Sauvage, J.-P. *J. Am. Chem. Soc.* **1997**, *117*, 4599–4607. (c) Albrecht-Gary, A. M.; Saad, Z.; Dietrich-Buchecker, C. O.; Sauvage, J.-P. *J. Am. Chem. Soc.* **1985**, *105*, 3205–3209. (d) Meyer, M.; Albrecht-Gary, A.-M.; Dietrich-Buchecker, C. O.; Sauvage, J.-P. *Inorg. Chem.* **1999**, *38*, 2279–2287. (e) Gumienna-Kontecka, E.; Rio, Y.; Bourgogne, C.; Elhabiri, M.; Louis, R.; Albrecht-Gary, A.-M.; Nierengarten, J.-F. *Inorg. Chem.* **2004**, *43*, 3200–3209. (f) Albrecht-Gary, A. M.; Blau, O.; Frohlichb, R. *Proc. Natl. Acad. Sci. U.S.A.* **2002**, *99*, 4867–4872.

(18) Ronson, T. K.; Adams, H.; Riis-Johannessen, T.; Jeffery, J. C.; Ward, M. D. *New J. Chem.* **2006**, *30*, 26–28.

(19) Argent, S. P.; Adams, H.; Riis-Johannessen, T.; Jeffery, J. C.; Harding, L. P.; Clegg, W.; Harringtond, R. W.; Ward, M. D. *Dalton Trans.* **2006**, 4996–5013.

(20) Xu, J.; Parac, T. N.; Raymond, K. N. *Angew. Chem., Int. Ed.* **1999**, *38*, 2878–2882.

(21) Tuna, F.; Hamblin, J.; Jackson, A.; Clarkson, G.; Alcock, N. W.; Hannon, M. J. *Dalton Trans.* **2003**, 2141–2148.

(22) Hannon, M. J.; Painting, C. L.; Jackson, A.; Hamblin, J.; Errington, W. *Chem. Commun.* **1997**, 1807–1808.

(23) (a) Carroll, R. L.; Gorman, C. B. *Angew. Chem., Int. Ed.* **2002**, *41*, 4378–4400. (b) Balzani, V.; Credi, A.; Venturi, M. *Chem.—Eur. J.* **2002**, *8*, 5525–5532. (c) Flood, A. H.; Stoddart, J. F.; Steuerman, D. W.; Heath, J. R. *Science* **2004**, *306*, 2055–2056. (d) Green, J. E.; Choi, J. W.; Boukai, A.; Bunimovich, Y.; Johnston-Halperin, E.; Delonno, E.; Luo, Y.; Sheriff, B. A.; Xu, K.; Shin, Y. S.; Tseng, H. R.; Stoddart, J. F.; Heath, J. R. *Nature* **2007**, *445*, 414–417.

(24) Schultz, D.; Biaso, F.; Shahi, A. R. M.; Geoffroy, M.; Rissanen, K.; Gagliardi, L.; Cramer, C. J.; Nitschke, J. R. *Chem.—Eur. J.* **2008**, *14*, 7180–7185.

(25) Pallavicini, P.; Boiocchi, M.; Dacarroa, G.; Manganoa, C. *New J. Chem.* **2007**, *31*, 927–935.

(26) Medlycott, E. A.; Hanan, G. S. *Chem. Commun.* **2007**, 4884–4886.

(27) Youinou, M.-T.; Ziessel, R.; Lehn, J.-M. *Inorg. Chem.* **1991**, *30*, 2144–2148.

(28) Yao, Y.; Perkovic, M. W.; Rillema, P.; Woods, C. *Inorg. Chem.* **1992**, *31*, 3956–3962.

(29) Kubas, J. G.; Monzyl, B.; Crumbliss, A. M. *Inorg. Synth.* **1990**, *28*, 68–70.

(30) Bernhard, S.; Takada, K.; Jenkins, D.; Abruña, H. D. *Inorg. Chem.* **2002**, *41*, 765–772.

The structure of the product was assessed by ^{1}H NMR and ^{13}C NMR in CD_3OD. Labels for the ligand protons are shown in Supporting Information, Figure S1. ^{1}H NMR (CD_3OD): δ/ppm 8.65 (d, 4H, J = 8.2 Hz), 8.17 (d, 4H, J = 8.9 Hz), 8.08 (d, 4H, J = 8.3 Hz), 8.00 (d, 4H, J = 8.9 Hz), 7.82 (d, 4H, J = 8.2 Hz), 7.29 (d, 4H, J = 8.3 Hz), 2.86 (m, 4H), 2.68 (m, 4H), 2.16 (s, 12H), 1.83 (m, 4H). ^{13}C NMR: δ/ppm 160.29, 158.24, 142.70, 137.58, 137.17, 127.79, 126.55, 126.34, 125.73, 124.44, 39.21, 27.73, 24.07.

[Cu(mphenpr)](ClO$_4$). The displacement of the equilibrium from $[Cu_2(mphenpr)_2](ClO_4)_2$ to $[Cu(mphenpr)](ClO_4)$ is complete in solutions heated above 90 °C. Ethoxyethanol was the preferred solvent where the formation of $[Cu(mphenpr)]^+$ gives a burgundy-red color to the solution. To obtain the crystals of $[Cu(mphenpr)](ClO_4)$, a concentrated solution of $[Cu_2(mphenpr)_2](ClO_4)_2$ in ethoxyethanol was heated to the boiling point (135 °C) and quickly chilled to freeze the equilibrium. Reformation of the $[Cu_2(mphenpr)_2]^{2+}$ in this solution at room temperature was followed by NMR. Because the reformation is a very slow process, crystals of $[Cu(mphenpr)](ClO_4)$ were obtained by the slow diffusion of ethyl ether into the chilled solution of $[Cu(mphenpr)](ClO_4)$. Anal. Calcd for $[Cu(C_{29}N_4H_{24})](ClO_4)$: H, 4.92; C, 70.78, N, 11.39. Found: H, 4.8; C, 71.1, N, 11.1. Mass spectrum parent peak m/z = 492.5 corresponding to $[Cu(mphenpr)]^+$ (F.W. = 492.08), The structure of the complex was established ^{1}H NMR and ^{13}C NMR in $CDCl_3$. ^{1}H NMR: δ/ppm 8.59 (d, 2H, H7,7′), 8.48 (d, 2H, H4,4′), 8.04 (s, 4H, H6,6′, H5,5′), 7.92 (d, 2H, H8,8′), 7,76 (d, 2H, H3,3′), 3.27 (m, 2H, Hb), 3.20 (m, 2H, Hb), 2.26 (s, 6H, Ha), 2.26 (under singlet, 2H, Hc). ^{13}C NMR (approximated values obtained from HSQC-ed and HMBC spectra) δ/ppm: 161,4(C,9,9′), 157.3(C,2,2′), 143.1-(C10,10′), 142.5(C11,11′), 138.3(C7,7′), 137.4(C4,4′), 127.7-(C12,12′), 127.4(C13,13′), 126.2(C5,5′,C6,6′), 125.9(C8,8′), 125.6(C3,3′), 35.7 (CH_2b), 32.5 (CH_2c), 25.9 (CH_3a).

Pulse-Radiolytic Procedures. Pulse radiolysis experiments were carried out with a model TB-8/16−1S electron linear accelerator. The instrument and computerized data collection for time-resolved UV−vis spectroscopy and reaction kinetics have been described elsewhere in the literature.[31,32] Thiocyanate dosimetry was carried out at the beginning of each experimental session. The details of the dosimetry have been reported elsewhere.[31−36] The procedure is based on the concentration of $(SCN)_2^-$ radicals generated by the electron pulse in a N_2O saturated 10^{-2} M SCN^- solution. In the procedure, the calculations were made with G = 6.13 and an extinction coefficient, ε = 7.58×10^3 M^{-1} cm^{-1} at 472 nm, for the $(SCN)_2^-$ radicals.[31,33] In general, the experiments were carried out with doses that in N_2 saturated aqueous solutions resulted in $(2.0 \pm 0.1) \times 10^{-6}$ M to $(6.0 \pm 0.3) \times 10^{-6}$ M concentrations of e^-_{sol}. In these experiments, solutions were prepared by the procedure indicated above for the photochemical experiments. The liquids were deaerated with streams of the O_2-free gas, N_2 or N_2O, required for the experiment. To radiolyze a fresh sample with each pulse, an appropriate flow of the solution through the reaction cell was maintained during the experiment. Other conditions used for the time-resolved spectroscopy of the reaction intermediates or in the investigation of the reaction kinetics are given in the Results section. Radiolysis with ionizing radiation of CH_3OH and CH_3OH/H_2O mixtures have been reported elsewhere in the literature.[33−35] These studies have shown that pulse radiolysis can be used as a convenient source of e^-_{sol} and $C^{\bullet}H_2OH$ radicals, Scheme 1.

Scheme 1

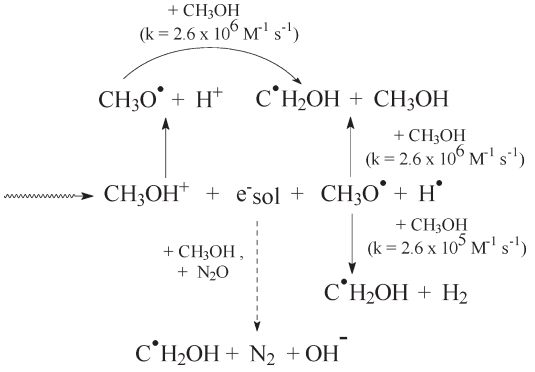

Since e^-_{sol} and $C^{\bullet}H_2OH$ have large reduction potentials, −2.8 V versus NHE for e^-_{sol} and −0.92 V versus NHE for $C^{\bullet}H_2OH$, they have been used for the reduction of coordination complexes and for the study of electron transfer reactions. The yield of e^-_{sol} in CH_3OH ($G \sim 1.1$),[33] is about one-third of the G-value in the radiolysis of H_2O ($G \sim 2.8$).[35] In solutions where e^-_{sol} was scavenged with N_2O, the $C^{\bullet}H_2OH$ radical is the predominant product (yield > 90%).

Reactions of e^-_{sol} with alkyl and aryl chlorocarbons in methanolic solutions were used for the cleavage of the chlorocarbons C−Cl bond that rapidly produces the corresponding C-centered alkyl and aryl radicals.[36] While the formation of the alkyl radicals is completed in less than 1 μs in 10^{-2} M chlorocarbon solutions, the reaction of the C-centered radicals with CH_3OH are very slow, $k \leq 10^3$ M^{-1} s^{-1}. Therefore, the C-centered radicals are exclusively scavenged by the Cu(I) complexes in the solution. The reactions of $[Cu^I_2(mphenpr)_2]^{2+}$ with e^-_{sol} or C-centered alkyl and aryl radicals were investigated over limited periods of time from the preparation of the solutions to the end of the pulse radiolysis experiment. These limited periods of time ensured that under a given medium condition there will be no interference from other species produced in parallel reactions such as the unfolding process.

The reaction kinetics were investigated by following the absorbance change at given wavelengths of the spectrum and incorporating those changes in the dimensionless parameter, $\xi = (\Delta A_{inf} - \Delta A_t)/(\Delta A_{inf} - \Delta A_0)$.[37] In ξ, ΔA_0 is the absorbance change at the beginning of the reaction, ΔA_t is determined at an instant t of the reaction, and ΔA_{inf} is determined at the end of the reaction.

Spectroscopic Measurements. UV−vis and NMR spectra were recorded with solutions deaerated with streams of N_2 or Ar gas. 1D- and 2D-NMR spectra were recorded from deuterated solution of the compounds (CD_3CN, $CDCl_3$, CD_3OD, C_6D_6) at 300 K on a Bruker Avance 400 spectrometer operating at 400.13 MHz for ^{1}H and 100.61 MHz for ^{13}C nucleus, and equipped with a 5 mm broadband inverse probe head incorporating a z-gradient coil. The chemical shifts (in ppm) for 1D ^{1}H and ^{13}C spectra are reported relative to tetramethylsilane and calibrated with respect to residual solvent protons (^{1}H) or the carbon signal of deuterated solvents (^{13}C). The number of scans in each experiment was dependent on the sample concentration.

Computational Methods. The computational study of the Cu transition metal complexes has been carried out using the density functional theory (DFT) methods implemented in

(31) Hug, G. L.; Wang, Y.; Schöneich, C.; Jiang, P. -Y.; Fessenden, R. W. *Radiat. Phys. Chem.* **1999**, *54*, 559–566.
(32) Thomas, S.; Ruiz, G. T.; Ferraudi, G. *Macromolecules* **2006**, *39*, 6615–6621.
(33) Getoff, N.; Ritter, A.; Schworer, F. *Radiat. Phys. Chem.* **1993**, *41*, 797–801.
(34) Dorfman, L. M. In *The Solvated Electron in Organic Liquids*; Gould, R. F., Ed.; Adv. Chem. Series, American Chemical Society: Washington, DC, 1965.
(35) Simic, M.; Neta, P.; Hayon, E. *J. Phys. Chem.* **1969**, *73*, 3794–3798.
(36) Buxton, G. V.; Greenstock, C. L.; Helman, W. P.; Ross, A. R. *J. Phys. Chem. Ref. Data* **1988**, *17*, 513–586.
(37) Frost, A. A.; Pearson, R. G. *Kinetics and Mechanism*; John Wiley & Sons: New York, 1953; Chapter 3, pp 28−31.

Gaussian 03.[38] DFT methods have been shown to reproduce the structural properties of several interesting transition metal centers, and their validity to model ground-state properties is widely accepted.[39−43] On this basis, they have been used to better assess the structural characteristics of the reaction intermediates, helping in this way to discern among possible reaction mechanisms. The systems studied herein were subjected to unrestrained energy minimizations using the B3LYP functional[44,45] with the 6-31+G* basis set[45] for nonmetal atoms and the Los Alamos effective core potentials (LANL2DZ)[46−48] for the metal. The basis set was chosen following a recently published study of the performance of different DFT methodologies/basis sets for the calculation of heats of formation of different systems containing third row transition metals.[49] The solvent has been modeled within a continuous approach (Polarizable Continuous Model, PCM)[50] in the study of the electronic characteristics and UV−vis spectra. Time dependent DFT (TDDFT) models were used to assign the nature of the observed electronic transitions.

Electrochemistry. Voltammetry experiments were carried out with an Autolab PGSTAT30 computer controlled potentiostat equipped with a three electrode electrochemical cell. The working electrode was platinum or glassy carbon, the auxiliary was platinum and the external reference was a saturated calomel connected through a solvent bridge to minimize contamination of the test solution. All samples were run under an Ar atmosphere with 0.10 M tetraethyl ammonium perchlorate as supporting electrolyte at 25 °C. The system was calibrated with a Fc^+/Fc internal standard, and all potentials are quoted relative to this couple.

X-ray Crystallography. The samples were mounted on a Kapton loop using Paratone-N hydrocarbon oil. For two structures, X-ray intensity data were recorded on a Bruker APEX-II[51] CCD area detector with graphite monochromated Mo−Kα radiation. The data were collected at a temperature of 100(2) K. Synchrotron data for the remaining structure were collected at Beamline 11.3.1 at the Advanced Light Source at Lawrence Berkeley National Laboratory. Data were recorded at a temperature of 150(2) K using the APEX-2 software suite on a Bruker APEX-II detector mounted on a D8 goniometer using radiation tuned to 0.7749 Å (17.000 keV) monochromated through a channel-cut SI-⟨111⟩ crystal. Frames corresponding to an arbitrary sphere of data were collected using a combination ω and φ-scans of 0.3°. Data were integrated by the program SAINT[52] and were corrected for Lorentz, polarization, and absorption effects based on a comparison of redundant and equivalent reflections using SADABS.[53] Data were analyzed for agreement, and the space group was determined using XPREP.[54] No decay correction was applied. The structure was solved by direct methods[55] and expanded using Fourier techniques.[56] Neutral atom scattering factors for the radiation used were determined from those of Kissel and Pratt (XDISP).[57] Non-hydrogen atoms were refined anisotropically. Hydrogen atoms were included in calculated positions but were not refined. More details of the data collections and structure refinements are presented in Table 1.

Table 1. Crystal and Refinement Data for $[Cu_2(mphenpr)_2](ClO_4)_2 \cdot CH_3CN$

compound	$[Cu_2(mphenpr)_2](ClO_4)_2 \cdot CH_3CN$
chemical formula	$C_{58}H_{48}Cu_2N_8$, $2(ClO_4)$, C_2H_3N
formula weight (g/mol)	1224.08
temperature, K	100(2)
crystal system	orthorhombic
space group	*Pbca* (No. 61)
crystal shape, color	needle, orange
a, Å	16.9255(4)
b, Å	25.2671(5)
c, Å	25.3322(6)
α, deg	90.0
β, deg	90.0
γ, deg	90.0
V, Å^3	10833.5(4)
Z	8
density (calculated), mg/mm^3	1.501
F(000)	5040
absorption coefficient, μ, mm^{-1}	0.951
θ range, deg	2.5 to 26.5
h, *k*, *l*	$-21 > h > 21$, $-29 > k > 31$, $-31 > l > 31$
reflections measured, $I > 2\sigma(I)$	8654
parameters	735
R1,[a] wR2[b] [$F^2 > 2\sigma(F^2)$]	R1 = 0.0385, wR2 = 0.0921
R1,[a] wR2[b] [all data]	R1 = 0.0577, wR2 = 0.1015

[a] $R1 = \sum||F_o| - |F_c||/\sum|F_o|$. [b] $wR2 = [\sum w(F_o^2 - F_c^2)^2/\sum w(F_o^2)^2]^{1/2}$.

Results and Discussion

The new binucleating ligand, 1,3-bis(9-methyl-1,10-phenanthrolin-2-yl)propane = mphenpr, provides a more rigid coordination sphere for the Cu(I) centers than other related binucleating ligands where bpy subunits are connected by a bridge.[58] Nevertheless, the mphenpr having a more flexible

(38) Frisch, M. J.; Trucks, G. W.; Schlegel, H. B.; Scuseria, G. E.; Robb, M. A.; Cheeseman, J. R.; Montgomery, Jr., J. A.; Vreven, T.; Kudin, K. N.; Burant, J. C.; Millam, J. M.; Iyengar, S. S.; Tomasi, J.; Barone, V.; Mennucci, B.; Cossi, M.; Scalmani, G.; Rega, N.; Petersson, G. A. ; Nakatsuji, H.; Hada, M.; Ehara, M.; Toyota, K.; Fukuda, R.; Hasegawa, J.; Ishida, M.; Nakajima, T.; Honda, Y.; Kitao, O.; Nakai, H.; Klene, M.; Li, X.; Knox, J. E.; Hratchian, H. P.; Cross, J. B.; Bakken, V.; Adamo, C.; Jaramillo, J.; Gomperts, R.; Stratmann, R. E.; Yazyev, O.; Austin, A. J.; Cammi, R.; Pomelli, C.; Ochterski, J. W.; Ayala, P. Y.; Morokuma, K.; Voth, G. A.; Salvador, P. Dannenberg, J. J.; Zakrzewski, V. G.; Dapprich, S.; Daniels, A. D.; Strain, M. C.; Farkas, O.; Malick, D. K.; Rabuck, A. D.; Raghavachari, K.; Foresman, J. B.; Ortiz, J. V.; Cui, Q.; Baboul, A. G.; Clifford, S.; Cioslowski, J.; Stefanov, B. B.; Liu, G.; Liashenko, A.; Piskorz, P.; Komaromi, I.; Martin, R. L.; Fox, D. J.; Keith, T.; Al-Laham, M. A.; Peng, C. Y.; Nanayakkara, A.; Challacombe, M.;. Gill, P. M. W.; Johnson, B.; Chen, W.; Wong, M. W.; Gonzalez, C.; Pople, J. A. *Gaussian 03*, revision C.02; Gaussian, Inc.: Pittsbourgh, PA, 2003.
(39) Harris, D. L. *Curr. Opin. Chem. Biol.* **2001**, *5*, 724–735.
(40) Noodleman, L.; Lovell, T.; Li, W.-G.; Han, J.; Himo, F. *Chem. Rev.* **2004**, *104*, 459–508.
(41) Solomon, E. I.; Szilagyi, R. K.; DeBeer, G. S.; Basumallick, L. *Chem. Rev.* **2004**, *104*, 419–458.
(42) Estiu, G. E.; Merz, K. *J. Phys. Chem.* **2007**, *111*, 10263–10274.
(43) Estiu, G. E.; Suarez, D.; Merz, K. *J. Comput. Chem.* **2006**, *27*, 1240–1262.
(44) Becke, A. D.; Yarkony D. R. In *Modern Electronic Structure Theory Part II*; World Scientific: Singapore, 1995.
(45) Hehre, W. J.; Radom, L.; Schleyer, P. V. R.; Pople, J. A. *Ab Initio Molecular Orbital Theory*; John Wiley & Sons: New York, 1986.
(46) Hay, P. J.; Wadt, W. R. *J. Chem. Phys.* **1985**, *82*, 270–283.
(47) Wadt, W. R.; Hay, P. J. *J. Chem. Phys.* **1985**, *82*, 284–298.
(48) Hay, P. J.; Wadt, W. R. *J. Chem. Phys.* **1985**, *82*, 299–310.
(49) Riley, K.; Merz, K. *J. Phys. Chem. A* **2007**, *111*, 6044–6053.
(50) Foresman, J. B.; Keith, T. A.; Wiberg, K. B.; Snoonian, J.; Frisch, M. J. *J. Phys. Chem.* **1996**, *100*, 16098–16104.
(51) *APEX-2 v2009−1: Suite for X-ray structure data collection and determination*; Bruker Analytical X-ray Systems, Inc.: Madison, WI, 2009.
(52) *SAINT: SAX Area-Dectector Integration Program*; Bruker Analytical X-ray Systems, Inc.: Madison, WI, 2009.
(53) *SADABS: Siemens Area Detector ABSorption correction program*; George Sheldrick, University of Göttingen: Göttingen, Germany, 2008.
(54) *XPREP* (*v 6.14*)*: Part of the SHELXTL Crystal Structure Determination Package*; Bruker Analytical X-ray Systems, Inc.: Madison, WI, 1995.
(55) *SHELXS: Program for the Solution of X-ray Crystal Structures*; George Sheldrick, University of Göttingen: Göttingen, Germany, 2008.
(56) *SHELXL: Program for the Refinement of X-ray Crystal Structures*; George Sheldrick, University of Göttingen: Göttingen, Germany, 2008.
(57) *XDISP: X-ray Anomalous Dispersion part of the WinGX package*; Kissel, L., Pratt, R. H. *Acta Crystallogr.* **1990**, *A46*, 170−175;Farrugia, L. J. *J. Appl. Crystallogr.* **1999**, *32*, 837–838.
(58) Fatin-Rouge, N.; Blanca, S.; Pfeil, A.; Rigault, A.; Albrecht-Gary, A.-M.; Lehn, J.-M. *Helv. Chim. Acta* **2001**, *84*, 1694–1711.

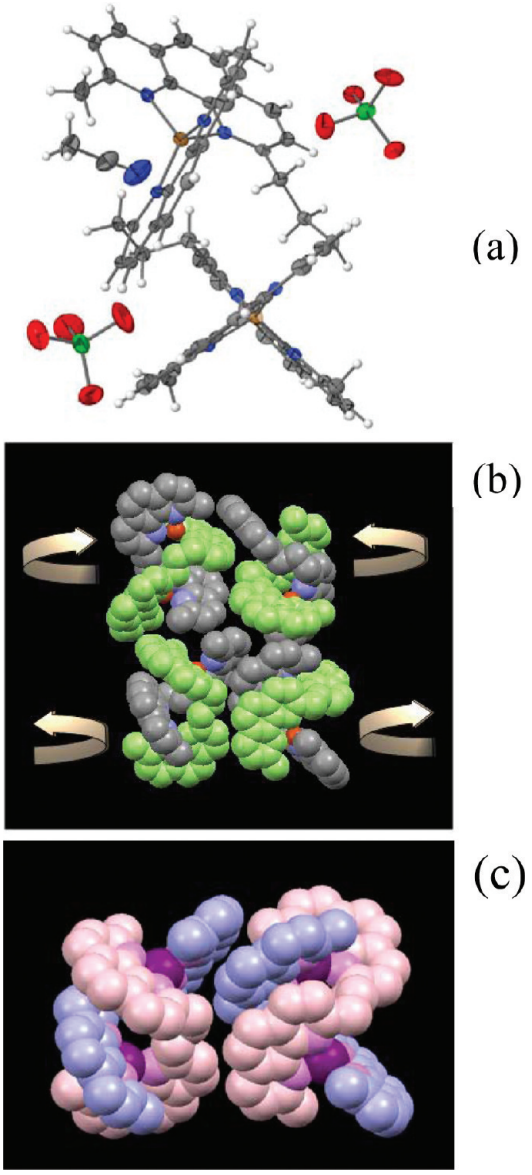

Figure 1. (a) Molecular structure of $[Cu^I_2(mphenpr)_2](ClO_4)_2$. Thermal ellipsoids are drawn at the 50% probability level. $[Cu^I_2(mphenpr)_2](ClO_4)_2$ crystallizes in the centric space group *Pbca* as a racemic mixture of chiral binuclear units with *M* or *P* helicity, (b) and (c).

propylene bridge than other triatomic bridges[9c] provided insights in the mechanism of the $[Cu^I_2(mphenpr)_2]^{2+}$ unfolding. In the unfolding of $[Cu^I_2(mphenpr)_2]^{2+}$, the experimental observations support the formation of a binuclear intermediate species, $\{[Cu^I_2(mphenpr)_2]^{2+}\}^*$, with a face-to-face isomer of the helicate[9c,d] or some other species with a partially dissociated Cu(I) center.[59] Accordingly, characterization of the system by X-ray, NMR, and computation work has been carried out to affirm the helical nature of the principal copper(I) complex and also to examine the related equilibria. The dimer $[Cu^I_2(mphenpr)_2]_2(ClO_4)_2$ dissociates in CH_3CN, CH_3OH, or CH_2Cl_2 solvents producing the monometallic Cu(I) complex, $[Cu^I(mphenpr)]^+$, in a reversible solvent dependent process. On the other hand, the addition of CCl_4 to the solution of the helicate leads to its oxidation to $[Cu^{II}(mphenpr)Cl]^+$.

(59) (a) Margerum, D. W. In *Substitution Reaction of Chelates*; ACS Symposium Series 198; American Chemical Society: Washington, DC, 1982; pp 3−38. (b) Cabbiness, D. K.; Margerum, D. W. *J. Am. Chem. Soc.* **1969**, *91*, 6540–6548.

Table 2. Selected Bond Distances (Å) and Bond Angles (deg) of $[Cu^I_2(mphenpr)_2](ClO_4)_2$ and $[Cu^I(Diphen)]_2(C1O_4)_2$[a]

	$[Cu^I_2(mphenpr)_2](ClO_4)_2$	$[Cu^I(Diphen)]_2(C1O_4)_2$
	Bond Distances [b]	
Cu−N(1)	2.043	1.992
Cu−N(2)	2.043	2.081
Cu−N(3)	2.037	2.026
Cu−N(4)	2.052	2.034
	Bond Angles [b]	
N(1)−Cu−N(2)	82.3	82.6
N(1)−Cu−N(3)	121.9	135.4
N(1)−Cu−N(4)	119.7	120.8
N(2)−Cu−N(3)	136.39	119.9
N(2)−Cu−N(4)	128.07	108.1
N(3)−Cu−N(4)	119.7	82.5

[a] Ligand abbreviated name, Diphen = 1,2-Bis(9-methyl-1,10-phenanthrolin-2-yl)ethane, and chrystallographic data from ref 28. [b] Equivalent atoms in $[Cu^I_2(mphenpr)_2](ClO_4)_2$ and $[Cu^I(Diphen)]_2(C1O_4)_2$ are numbered as in ref 28 for the sake of comparison.

Solid and Solution Phase Structure of $[Cu^I_2(mphenpr)_2]^{2+}$. A crystallographic structure of the helical dimer $[Cu^I_2(mphenpr)_2](ClO_4)_2$, Figure 1a, was determined using a crystal formed from a racemic sample. The X-ray structural analysis indicates that $[Cu^I_2(mphenpr)_2]^{2+}$ has a binuclear structure organized around the core of two Cu(I) centers. Two pairs of bidentate ligands joined by a propylene bridge define a geometry consisting of four N atoms in a flattened tetrahedron around each Cu center. Whereas both chelating N atoms of a phen unit bind to the same Cu(I) center, the propylene spacer, together with offset $\pi-\pi$ stacking interactions between the ligands generate a supramolecular double-strand helicate structure. It crystallizes in the centric space group *Pbca* as a racemic mixture of chiral binuclear units with *M* or *P* helicity, Figure 1b and c. The bond distances and bond angles in the structures of the $[Cu^I_2(mphenpr)_2](ClO_4)_2$ and the ethylene-bridged homologue[28] are shown in Table 2. While similar trends in bond distances exist in both structures, dissimilarities between bond angles can be attributed to differences in the stress associated with each bridge. A strong intramolecular $\pi-\pi$ overlap between two phen units of different ligands (closest interplanar distance 3.37 Å, Supporting Information, Figure S2a) may play an important role in stabilizing the binuclear cation. Deviation from a parallel arrangement of the planes of two 9-methyl-1,10-phenanthrolin-2-yl (mphenoliyl) is noticed, Supporting Information, Figure S2b, and can also be rationalized by steric restrictions imposed by the propylene bridges. It can be triggered otherwise by the crystallization of a CH_3CN molecule in a pocket of the complex. To resolve this issue, modeling calculations were carried out.

The helicate structure was modeled by means of geometry optimizations starting from the crystallographic coordinates from which the cocrystallized solvent was deleted. The optimized structure, Figure 2a, shows the same deviation from planarity of interacting π-systems, suggesting that rather than induced by the solvent it may be triggered by the strain introduced in the structure by

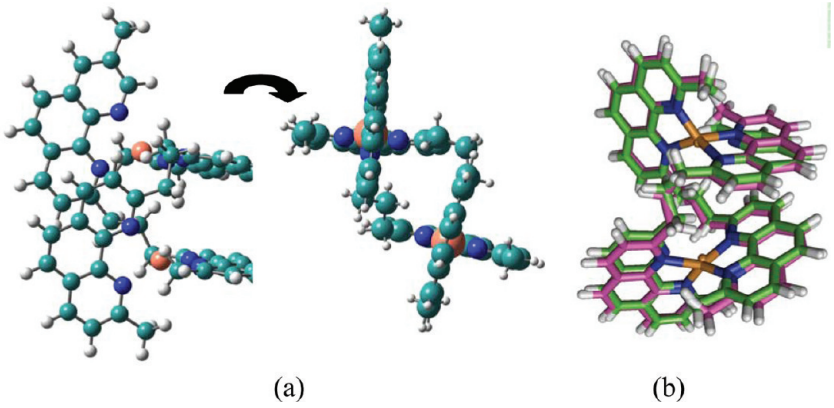

Figure 2. DFT optimized structure of the $[Cu^{I}_2(mphenpr)_2]^{2+}$ helicate, (a). Two views are shown, corresponding to a 90° rotation around a *z* axis. Color code as follows: C cyan, N blue, Cu orange. (b) Superposition of the DFT optimized (purple) and X-ray (green) structures of the $[Cu^{I}_2(mphenpr)_2]^{2+}$ helicate.

the propylene bridges. The superposition of the optimized and crystallized structures, Figure 2b, shows an outstanding coincidence. The bond distances of the ligands agree within 0.01 Å, with the largest deviation found for the calculated Cu−N distances, which are 0.1 Å longer than the experimental ones.

In solution, 1D NMR (^1H, ^{13}C), 2D NMR (COSY, NOESY, HSQC-ed, HMBC spectroscopies were also used for the characterization of the mphenpr ligand and the complex, $[Cu^{I}_2(mphenpr)_2]^{2+}$. For the free ligand, signals in the ^1H NMR of mphenpr in $CDCl_3$, Supporting Information, Figure S1, correspond to the aliphatic protons of the propylene bridge of the dimeric ligand and the aromatic protons of the 9-methyl-1,10-phenantrolin-2-yl groups. A triplet, Hb, is the signal of four methylenic protons adjacent to the phenanthroline in the propylene bridge. A quintuplet, Hc, corresponds to the protons of the central methylene group in the bridge. The NOESY spectra in $CDCl_3$ or CH_3OD show a correlation between the protons of the two 9-methyl-1,10-phenantrolin-2-yl groups in a weak dimer $(mphenpr)_2$, that is, H3−H8, H4−H7, Ha−Hb, Ha−Hc, which originates from a face to face superposition of two molecules of mphenpr, Supporting Information, Figure S3. As in the case of the solid, the $(mphenpr)_2$ configuration is probably stabilized by $\pi-\pi$ interactions between the two units of mphenpr. Proton interactions characteristic of the $(mphenpr)_2$ in the NOESY spectrum were lost when the solutions of mphenpr contained D_6-benzene. The splitting of the triplet signal of the methylene protons, Hb in Supporting Information, Figure S1, in two multiplet signals is consistent with the loss of equivalence between the protons of each methylene group. This splitting is characteristic of the NMR spectrum of complexes with a helical structure. NOESY couplings between H7−H6 and H7−H5 reveal the interaction between protons of different dimeric chains and confirm a helical configuration in solution, characterized by a parallel or near parallel arrangement of 9-methyl-1,10-phenantrolin-2-yl groups of different dimeric-ligands.

The helical structure of $[Cu^{I}_2(mphenpr)_2]^{2+}$ in the crystal, Figure 1, is conserved in CH_3OD according to mono and bidimensional NMR spectroscopy Supporting Information, Figure S4. The crystallization with a CH_3CN molecule, already shown in Figure 1, could be translated into strong solvent-complex interactions that drive the thermal transformations described in the next section.

Unfolding of the Helicate in Solution Phase. The electronic spectrum of deaerated solutions containing 2.0×10^{-4} M $[Cu^{I}_2(mphenpr)_2]^{2+}$ in either CH_3CN, CH_2Cl_2, or CH_3OH, kept in the dark and at room temperature, changes with time, Figure 3a. An equilibrium, eq 1, between the binuclear helicate and $[Cu^{I}(mphenpr)]^{+}$ accounts for the changes in the spectrum.

The formation of the $[Cu(mphenpr)]^{+}$ species was investigated by IR and ^1H NMR spectroscopies. Figure 3b shows the ^1H NMR spectrum of a 10^{-4} M solution of the helicate in CD_3CN recorded with different delays after the preparation of the solution. A decrease in the intensity of the six doublets of the aromatic protons in the ligands of $[Cu^{I}_2(mphenpr)_2]^{2+}$ and the appearance of the resonances of the protons of the ligand in $[Cu(mphenpr)]^{+}$ are consistent with the equilibrium shown in eq 1.

$$[Cu_2{}^{I}(mphenpr)_2]^{2+} \overset{K}{\rightleftharpoons} 2[Cu^{I}(mphenpr)]^{+} \qquad (1)$$

The equilibrium constant, K_T in eq 2, was evaluated by measuring the integrated ^1H NMR signals of the helicate and $[Cu(mphenpr)]^{+}$ in equilibrium, Supporting Information, Figure S5.

$$K_T = \frac{[[Cu^{I}(mphenpr)]^{+}]^2}{[[Cu_2{}^{I}(mphenpr)_2]^{2+}]} = 1.5 \times 10^{-3}\ \text{M} \qquad (2)$$

Different concentrations of $[Cu^{I}_2(mphenpr)_2]^{2+}$ complex between 5×10^{-4} and 1.0×10^{-3} M were used in the preparation of the solutions in CH_3OH, which were kept in the dark until the equilibration was attained. The optical spectrum of $[Cu^{I}(mphenpr)]^{+}$ was then obtained from the spectrum of the $[Cu^{I}_2(mphenpr)_2]^{2+}$ solution aged more than 3000 min, Figure 3a, and the concentrations of the bi- and mononuclear complexes estimated on the basis of K_T. Crystals of $[Cu^{I}(mphenpr)]ClO_4$ were isolated from an aged solution of $[Cu^{I}_2(mphenpr)_2]^{2+}$ in ethoxyethanol but unfortunately, these were not of X-ray quality. The UV−vis spectrum of the isolated $[Cu^{I}(mphenpr)]ClO_4$ agreed with the spectrum in Figure 3a providing support to the NMR-derived conclusions and

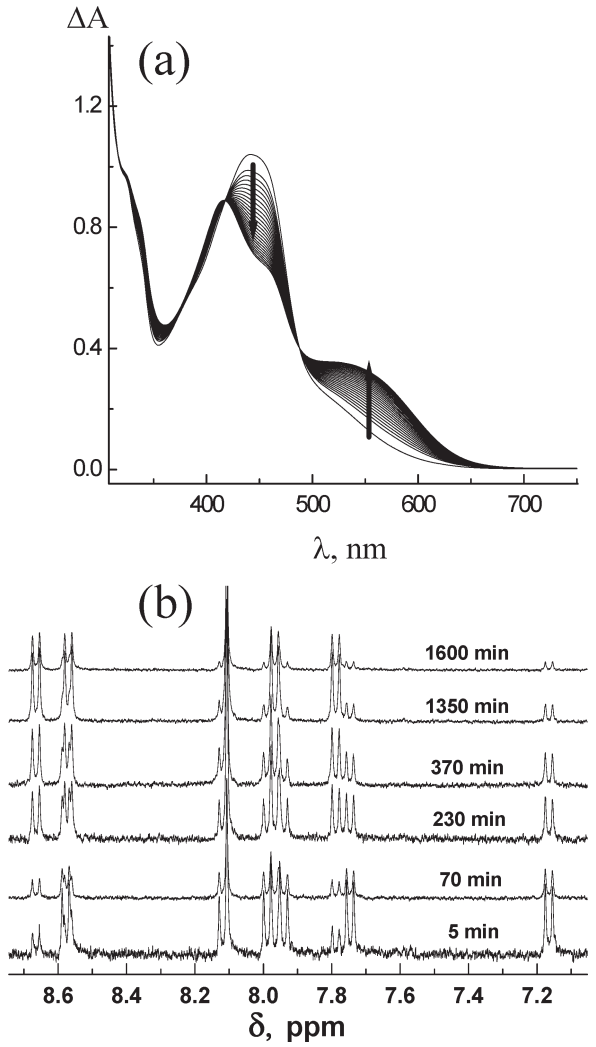

Figure 3. Unfolding of $[Cu^{I}_2(mphenpr)_2]^{2+}$. (a) Time-resolved changes in the spectrum of 1.0×10^{-4} M $[Cu^{I}_2(mphenpr)_2]^{2+}$ in CH_3OH. The spectra was automatically recorded at 10 min intervals. Arrows are indicative of the sense of the absorbance change. (b) ^1H NMR spectra recorded with different delays from the preparation of the solution.

confirming that the product of the equilibrium is $[Cu^{I}(mphenpr)]^{+}$. The spectrum of $[Cu^{I}_2(mphenpr)_2]^{2+}$ shows an absorption band at 445 nm while the spectrum of the monomer ($[Cu^{I}(mphenpr)]^{+}$) shows two bands ($\lambda_{max} = 415$ and 530 nm) and a shoulder ($\lambda \sim 500$ nm).

In the absence of X-ray structural information, electronic structure calculations were used to further elucidate the nature of $[Cu^{I}(mphenpr)]^{+}$ in the proposed equilibrium. The calculated structure of the mononuclear complex, $[Cu^{I}(mphenpr)]^{+}$, was optimized at the same level of theory as the binuclear complex, and the electronic transitions were assigned following TDDFT calculations. The optimized geometries of the mono and binuclear structures, overlapped in Figure 4a, show how the ligand folds to coordinate the four nitrogen atoms to a single Cu(I) center. This coordination triggers a larger distortion from tetrahedral symmetry. The interplanar ligand angle, 90° in a tetrahedron, is reduced to 69° in $[Cu^{I}(mphenpr)]^{+}$. The metal-to-ligand charge-transfer (MLCT) d→π transition is calculated for the helicate dimer at 434 nm, with a shoulder at 397 nm originated

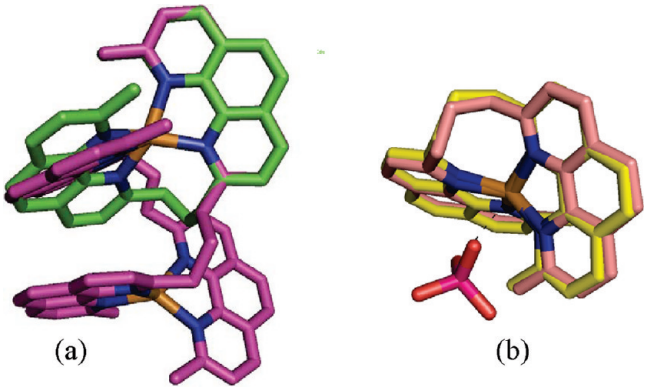

Figure 4. (a) DFT optimized structures of the $[Cu^{I}_2(mphenpr)_2]^{2+}$ helicate (purple) and the $[Cu^{I}(mphenpr)_2]^{+}$ monomer (green). One Cu center and the adjacent phen ligand of the structures are superimposed to highlight the coordination change. (b) DFT optimized structures of the $[Cu^{I}(mphenpr)_2]^{+}$ monomer: pink in vacuum, yellow with a ClO_4^{-} specifically coordinated (Cu−O distance 3.13 A). No distortion from the tetrahedral structure after ClO_4^{-} coordination becomes apparent. H atoms are omitted for clarity.

in similar excitations to higher lying π orbitals. The band decreases in intensity after dissociation to the more distorted monomer, shifting to 399 nm while a second peak develops, calculated at 515 nm, with half the intensity of the 399 nm peak. Both peaks are associated with d→π transitions, HOMO-1→LUMO and HOMO→LUMO+1, respectively. The band at 434 nm in the dimer involves excitations from the four higher energy occupied to the four lowest energy unoccupied orbitals, d-centered, with some delocalization in the π system. Because of delocalization, these orbitals are close in energy, lying within bands of 0.0036 and 0.0026 hartree, occupied and virtual orbitals, respectively. The dissociation to the monomer splits the energy of the HOMO, HOMO-1 orbitals in 0.02687 hartree, resulting in a splitting of the band and in the observed red and blue shifts. No band at 550 nm results from the calculation of the monomer, but it does develop, with a peak at 569 nm, when a solvent molecule is modeled specifically coordinated to the Cu center. As will be further discussed, both $Cu^{II}-Cl^{-}$ and $Cu^{II}-OClO_3^{-}$ coordination has been found in the crystallographic data of the oxidized monomeric species ($[Cu^{II}(mphenpr)]^{2+}$). By analogy, a -$OClO_3^{-}$ has been modeled coordinated to the $[Cu^{I}(mphenpr)]^{+}$ monomer, and the geometry was optimized starting from the X-ray coordinates of the oxidized complex. The distorted tetrahedral structure is conserved with no apparent change, Figure 4b. This is not surprising given the Cu−O distance (3.13 Å) at which the -$OClO_3^{-}$ is stabilized. Nevertheless, this weak coordination influences the electronic density and consequently the position of the bands. For the $\{[Cu^{I}(mphenpr)]^{+}\ ClO_4^{-}\}$ complex, the TDDFT calculations gave bands at 419 and 569 nm, resulting from d→π transitions; HOMO-1→LUMO and HOMO→LUMO, LUMO+1, respectively. Whereas the HOMO is centered in the Cu d system, the HOMO-1 has also some electron density on the π-orbitals of the coordinated ClO_4^{-}. The near degenerate LUMO, LUMO+1 are centered on each of the phenanthroline moieties. A shoulder at 500 nm is originated in similar transitions from the HOMO, d-centered, to the LUMO+2, LUMO+3, with π-density on each of the

phen moieties. The perfect agreement between the experimentally determined transitions and those calculated for the $\{[Cu^{I}(mphenpr)]^{+}\ ClO_4^{-}\}$ complex indicates that the coordination found in the crystal for the oxidized monomer is weakly stabilized in solution in the early stages of the dissociation.

Electrochemistry. The voltammetric behavior of the helicate dimer species is complicated by the slow, solvent dependent, interconversion involving the monomer−dimer equilibrium. Studies were carried out in a number of different solvents, and potentials were referenced to the Fc^{+}/Fc couple and calibrated with the behavior of $[Cu(dmp)_2]^{2+/+}$. A typical voltammogram for a sample of the helicate dimer in CH_3CN solvent is shown in Supporting Information, Figure S6. Two processes are noted. The dominant process is a quasi-reversible two-electron change around 0.34 V ascribed to the helicate. Simulation indicates that the two processes differ in potential by less than 10 mV demonstrating that the copper centers are effectively independent. The minor process at 0.01 V increases with time and is also quasi-reversible but corresponds to a single-electron transfer for the monomeric species. Confirmation comes from experiments where an independent sample of the monomer is used, in which case it is the helicate dimer signal that increases with time. This behavior is very similar to that presented by Yao for the $[Cu_2(mphenet)_2]^{2+}$ complex, where mphenet = 1,3-bis(9-methyl-1,10-phenanthrolin-2-yl)ethane.[28] While the potential for reduction of the helicates, $[Cu_2(mphenet)_2]^{4+}$ and $[Cu_2(mphenpr)_2]^{4+}$, are very similar, the potentials for reduction of the monomeric complexes vary considerably. $[Cu(mphenet)]^{2+}$ has the lowest reduction potential, −0.13 V, with the two phen groups constrained by the CH_2-CH_2 bridge, a geometric restriction that prevents the adoption of a tetrahedral arrangement of ligand donors preferred by copper(I). $[Cu(mphenpr)]^{2+}$ with its more flexible bridge is more readily reduced, and the potential is intermediate between the potential for $[Cu(mphenet)]^{2+}$ and the potential for reduction of the unconstrained $[Cu(dmp)_2]^{2+}$ at 0.28 V.

Equilibration Kinetics. The equilibration process shown in eq 1 occurred in two steps with a solvent-dependent rate that increased in the order $CH_3CN > CH_2Cl_2 > CH_3OH$, Supporting Information, Figure S7. Solutions of $[Cu^{I}_2(mphenpr)_2]^{2+}$ in CH_3CN having concentrations of the helicate between 1×10^{-3} and 1×10^{-4} M were used in a study of the dependence of the reaction kinetics on complex concentration. On the basis of the rate of equilibration in these solutions, eqs 3, 4 account for the experimental observations.

$$[Cu^{I}_2(mphenpr)_2]^{2+} \rightleftarrows \{[Cu^{I}_2(mphenpr)_2]^{2+}\}* \quad (3)$$

$$\{[Cu^{I}_2(mphenpr)_2]^{2+}\}* \rightleftarrows 2[Cu^{I}_2(mphenpr)]^{+} \quad (4)$$

A lifetime, $\tau = 15$ min, independent of complex concentration was recorded for the first step of the process in CH_3CN. This is the expected result when both the forward and backward reactions of the equilibration, eq 3, are kinetically first order. It implies, therefore, that an intermediate, $\{[Cu^{I}_2(mphenpr)_2]^{2+}\}*$, is formed and that $\{[Cu^{I}_2(mphenpr)_2]^{2+}\}*$ must also be a binuclear Cu(I) species. In contrast, the second step of the process exhibited a lifetime with a strong dependence on the initial $[Cu^{I}_2(mphenpr)_2]^{2+}$ concentration, namely, $\tau = 737$, 334, and 266 min for the corresponding concentrations 1×10^{-4} M, 2×10^{-4} M, and 4×10^{-4} M. This dependence of the lifetime on the initial $[Cu^{I}_2(mphenpr)_2]^{2+}$ concentration is the outcome of second order kinetics of the reverse reaction in eq 4.

The proposed mechanism, eqs 3, 4, was verified by fitting the time-resolved change of the 445 nm absorbance to the set of eqs 5−7.

$$\frac{d[[Cu^{I}_2(mphenpr)_2]^{2+}]}{dt} = -k_3[[Cu^{I}_2(mphenpr)_2]^{2+}] + k_{-3}[\{[Cu^{I}_2(mphenpr)_2]^{2+}\}*] \quad (5)$$

$$\frac{d[\{[Cu^{I}_2(mphenpr)_2]^{2+}\}*]}{dt} = k_2[[Cu^{I}_2(mphenpr)_2]^{2+}] - (k_{-2} + k_3)[\{[Cu^{I}_2(mphenpr)_2]^{2+}\}*] + k_{-3}[[Cu^{I}(mphenpr)]^{+}]^2 \quad (6)$$

$$\frac{d[[Cu^{I}(mphenpr)]^{+}]}{dt} = 2k_4[\{[Cu^{I}_2(mphenpr)_2]^{2+}\}*] - 2k_{-4}[[Cu^{I}(mphenpr)]^{+}]^2 \quad (7)$$

In eqs 5−7, k_3, k_{-3}, k_4, and k_{-4} are respectively the rate constants of the forward and reverse reactions in eqs 3, 4. Given the large difference in the lifetimes of the first and second step, it was assumed that for times longer than 45 min, namely, more than three times the lifetime of the first step, the $[Cu^{I}_2(mphenpr)_2]^{2+}$ and the intermediate species $\{[Cu^{I}_2(mphenpr)_2]^{2+}\}*$ were in equilibrium, and changes in the spectrum of the solution were controlled by the relaxation of eq 4. Equations 5−7 were numerically integrated with trial values of the rate constants until a set of values were found that provided a good description of the time dependence of the absorbance at $\lambda = 435$ nm. A good fit of the time-resolved changes in the UV−vis spectrum was obtained with the rate constants $k_3 = 1.0 \times 10^{-3}\ s^{-1}$, $k_{-3} = 3.3 \times 10^{-4}\ s^{-1}$, $k_4/k_{-4} = 4 \times 10^{-4}$ M. The reaction rate constant can be calculated, $k_3 + k_{-3} = 1.33 \times 10^{-3}\ s^{-1}$, and leads to a lifetime $\tau =$ 12.5 min, in agreement with the experimental observation ($\tau = 15$ min).

The dependencies of the $[Cu^{I}_2(mphenpr)_2]^{2+}$, $\{[Cu^{I}_2(mphenpr)_2]^{2+}\}*$, and $[Cu(mphenpr)]^{+}$ concentrations on time and on the initial $[Cu^{I}_2(mphenpr)_2]^{2+}$ concentration, $[Cu^{I}_2(mphenpr)_2]^{2+}{}_{t=0}$, were modeled on the basis of the experimentally obtained rate constants, Supporting Information, Figure S8. The results of the calculations agree with the experimentally determined concentrations of these species. Also, the values of the concentrations were calculated as a function of time, Supporting Information, Figure S9. The results accounted well for the dependence of the UV−vis spectrum on $[Cu^{I}_2(mphenpr)_2]^{2+}{}_{t=0}$.

An equilibrium constant for eq 3, $K_3 = 3$, was calculated from the corresponding forward and reverse reaction rate

constants. The overall equilibrium constant calculated as the product,

$$K_T = K_3 \frac{k_4}{k_{-4}} = 1.2 \times 10^{-3}\ \mathrm{M} \qquad (8)$$

is very close to the value calculated for the equilibrium constant, $K_T = 1.5 \times 10^{-3}$ M, of eq 2 using the ratio of the integrated signals of the NMR spectra. It is also in the range of equilibrium constants found for related Cu(I) helicate complexes.[4,60] Furthermore, a good agreement was found between the $[Cu^I_2(mphenpr)_2]^{2+}$ concentrations calculated from changes in the UV−vis spectrum of the solution and those concentrations calculated from the ^{1}H NMR spectra.

As noted above, eqs 3, 4 account for the rate of equilibration between the various Cu(I) species. The kinetic data led us to conclude that the intermediate $\{[Cu^I_2(mphenpr)_2]^{2+}\}^*$ is a binuclear Cu(I) complex participating in the rate determining step of the equilibration. It is improbable that $\{[Cu^I_2(mphenpr)_2]^{2+}\}^*$ forms the monomer $[Cu(mphenpr)]^+$ in a single step as represented in eq 4. Other species with partially dissociated ligands such as $[Cu^I(mphenpr)_2]^+$ may be rapidly formed and act as intermediates in the conversion of $\{[Cu^I_2(mphenpr)_2]^{2+}\}^*$ to $[Cu(mphenpr)]^+$.[61]

It is apparent from the experimental observations that the rate of the equilibration, from $[Cu^I_2(mphenpr)_2]^{2+}$ to $\{[Cu^I_2(mphenpr)_2]^{2+}\}^*$, is affected by the solvent. A comparison of the process in CH_3CN, CH_3OH, and CH_2Cl_2 shows that the solvent plays a complex role. Coordination of solvent with the copper(I) centers will assist the unwrapping of the mphenpr ligand around the Cu(I) centers. The role of the solvent has also been discussed by Raymond and collaborators,[20] giving significant relevance to the presence of an encapsulated "guest" solvent molecule in the equilibrium between the helicate and its face-to-face isomer. It is noteworthy that $[Cu^I_2(mphenpr)_2](ClO_4)_2$ crystallizes with a "guest" CH_3CN molecule in a pocket of the complex, and possible explanations for the observation that the initial intermediate $\{[Cu^I_2(mphenpr)_2]^{2+}\}^*$ in the reaction to form monomer is a binuclear species is that it corresponds to a face-to-face isomer or some other species with a partially dissociated Cu(I) center.

Oxidation of $[Cu^I_2(mphenpr)_2]^{2+}$ by CCl_4. The only process observed in the halocarbon solvents CH_3Cl and CH_2Cl_2 is the unfolding of the helicate. In contrast, the oxidation of $[Cu^I_2(mphenpr)_2]^{2+}$ was observed in solutions containing CCl_4. The time scale of the oxidation is long, allowing the process to be followed conveniently by changes in the UV−vis spectrum.

The absorption spectrum of the complex in deaerated CH_3CN or CH_3OH containing 0.1 to 1 M CCl_4, Figure 5, evolves over time, developing bands in the NIR (λ_{max} = 790 and 950 nm) which are characteristic of $[Cu^{II}(mphenpr)]^{2+}$. A bleaching of the $[Cu^I_2(mphenpr)_2]^{2+}$ MLCT absorption band is observed in the 350−600 nm region. The fact that the bleach of the MLCT absorption band of $[Cu^I_2(mphenpr)_2]^{2+}$ decreases without changing shape indicates that CCl_4 reacts with $[Cu^I_2(mphenpr)_2]^{2+}$ without forming any long-lived precursor of the $[Cu^{II}(mphenpr)]^{2+}$ product.

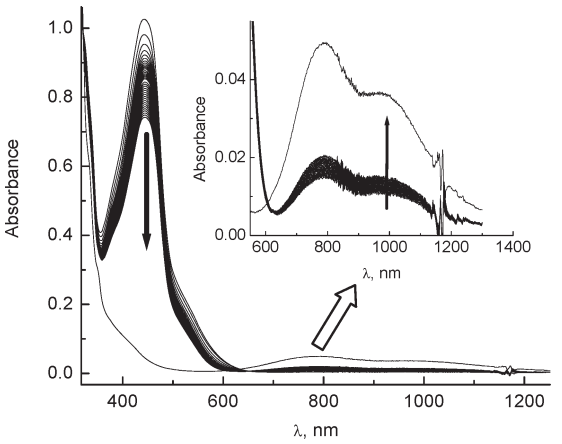

Figure 5. Time-resolved changes in the UV−vis absorption spectrum of a deaerated 1.0×10^{-4} M $[Cu^I_2(mphenpr)_2]^{2+}$ in a 10% (v:v) CCl_4 in CH_3CN mixed-solvent. The spectra were automatically recorded at 10 min intervals with the exception of the final three spectra. The final three spectra were recorded with delays of 2500, 7000, and 8600 min from the beginning of the reaction. Arrows are indicative of the sense of the absorbance change. The inset is an expanded view of the changes in the spectrum between 550 and 1400 nm.

The copper(II) product derivative was isolated and identified by X-ray crystallography. $[Cu^{II}(mphenpr)Cl]ClO_4$ crystallizes with a Cl^- counterion bound to the metal center, at a Cu−Cl distance of 2.35 Å and compares with the $[Cu^{II}(mphenpr)OClO_3]ClO_4$ formed directly from the reaction of $Cu(ClO_4)_2$ and the mphenpr ligand where there is a ClO_4^- counterion bound to the metal center with a Cu−O distance of 2.69 Å, Figure 6a. To confirm the assignment of the NIR bands, the geometry was optimized for the oxidized monomer with and without the bonded counterions. Both the $[Cu^{II}(mphenpr)]^{2+}$, the $[Cu^{II}(mphenpr)Cl]^+$, and the $[Cu^{II}(mphenpr)(ClO_4)]^+$ structures nicely overlap with the crystallographic structures, Figure 6. The comparison of the X-ray and optimized structures shows that the weakly bonded anions do not distort the geometry of the complex. The calculated UV−vis spectrum for the oxidized mononuclear complex with no attached counterion shows that the weakly bonded anions do not distort the geometry of the complex. The calculated UV−vis spectrum for the oxidized mononuclear complex with no attached counterion shows bands of very low intensity at 1107, 956, 790 nm associated with ligand-to-metal charge transfer (LMCT) transitions from π-orbitals to the d-centered singly occupied molecular orbital (SOMO), together with d → d transitions at 740, 690, and 650 nm. A band of higher intensity at 399 nm is also originated in a LMCT transition and is 10 times less intense than the one calculated at 433 nm for the binuclear complex, justifying the bleaching in this region of the spectrum.

The kinetics of the $[Cu^I_2(mphenpr)_2]^{2+}$oxidation was investigated following changes in the absorption spectrum

(60) Lange, J.; Elias, H.; Paulus, H.; Müller, J.; Weser, H. *Inorg. Chem.* **2000**, *39*, 3342–3349.

(61) Conductimetric measurements were also applied to the study of the equilibration process. The conductance of a 10^{-4} M $[Cu^I_2(mphenpr)_2]^{2+}$ solution in CH_3CN decreased monotonically in a 0 to 300 min time scale. The kinetics of the conductance change is therefore different of the one established by means of the absorption spectrum. A tentative interpretation of these experimental observations requires either or both that ClO_4^- and the reaction products form adducts, either weak complexes or neutral ion pairs, and that the products have a lesser mobility than $[Cu^I_2(mphenpr)_2]^{2+}$.

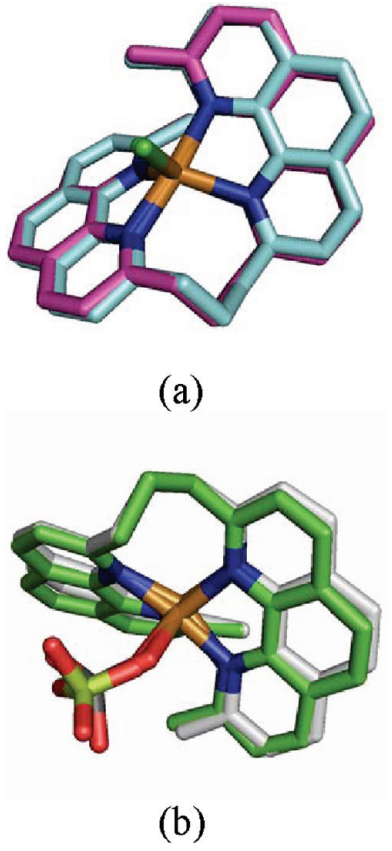

Figure 6. Superposition of the DFT optimized $[Cu^{II}(mphenpr)]$ (yellow) and $[Cu^{II}(mphenpr)(ClO_4)]^+$ (white) structures with the X-ray (green) $[Cu^{II}(mphenpr)(ClO_4)]^+$ structure of the oxidized monomer. H atoms are omitted for clarity. Other structural features are discussed in the text.

of a solution containing 1.0×10^{-4} M helicate and 1.0 M CCl_4 in CH_3CN. Both the disappearance of the MLCT absorption band of $[Cu^I_2(mphenpr)_2]^{2+}$ and the growth of the $[Cu^{II}(mphenpr)]^{2+}$ absorption bands exhibited biphasic kinetics. The first step of the process takes place in a time scale shorter than 1 h. Changes in the absorbance were fit to a single exponential with a lifetime, $\tau \sim 25$ min, that is slightly longer than the lifetime, $\tau \sim 15$ min, found for the relaxation of the equilibrium between $[Cu^I_2(mphenpr)_2]^{2+}$ and $\{[Cu^I_2(mphenpr)_2]^{2+}\}^*$ in neat CH_3CN, eq 3. Therefore, CCl_4 must be reacting with either one or both $[Cu^I_2(mphenpr)_2]^{2+}$ and $\{[Cu^I_2(mphenpr)_2]^{2+}\}^*$ during the first step of the process. To investigate the roles of $\{[Cu^I_2(mphenpr)_2]^{2+}\}^*$ in the first step of the reaction, two solutions of $[Cu^I_2(mphenpr)_2]^{2+}$ in CH_3CN were aged respectively 15 min (solution *a*) and 1 min (solution *b*) before the addition of a volume of CCl_4 that brought the concentrations to 1.0×10^{-4} M in the copper(I) complex and 1 M in the halocarbon. As a result of the aging, the concentration of intermediate $\{[Cu^I_2(mphenpr)_2]^{2+}\}^*$ was larger in solution *a* than in solution *b* at the time of the CCl_4 addition. A comparison of the reaction kinetics in both solutions shows that the first step is faster and persists a longer time in solution *a*, Supporting Information, Figure S10. The first step of the process was associated therefore with the generation of concentrations of $\{[Cu^I_2(mphenpr)_2]^{2+}\}^*$ and $[Cu^I(mphenpr)]^+$ via eqs 3, 4 large enough to reach a steady state regime. The second step of the process is much slower than the first step, and it was fit to an exponential function with a lifetime of $\tau \sim 1.4 \times 10^3$ min. It is consistent with the oxidation of the complex under the steady state regime in the species $\{[Cu^I_2(mphenpr)_2]^{2+}\}^*$ and $[Cu^I(mphenpr)]^+$.

The reduction of CCl_4 by copper(I) species can lead to the formation of $C^{\bullet}Cl_3$ radicals or CCl_4^- carbanions.[62−64] The ESR procedure of Chateauneuf et al.[65] allowed us to confirm the generation of $C^{\bullet}Cl_3$ radicals. TEMPO was used as a spin trap in deaerated and aerated solutions containing 1.0×10^{-3} M $[Cu^I_2(mphenpr)_2]^{2+}$, 1.0×10^{-3} M TEMPO, and 1.0 M CCl_4 in CH_3CN. In the deaerated solution, the disappearance of the TEMPO ESR resonances occurs simultaneously with the appearance of the Cu(II) species because of the coupling of the $C^{\bullet}Cl_3$ radical to the TEMPO nitroxyl group. The TEMPO ESR spectrum remained unaffected during the reaction of $[Cu^I_2(mphenpr)_2]^{2+}$ with CCl_4 in the aerated solution. This is the consequence of the fast scavenging of $C^{\bullet}Cl_3$ by O_2 to form $CCl_3OO^{\bullet}$ radicals that do not react with TEMPO.

Pulse radiolysis experiments were carried out with the aim of establishing the fate of the $C^{\bullet}Cl_3$ radicals in the presence of $[Cu^I_2(mphenpr)_2]^{2+}$. The reaction of $C^{\bullet}Cl_3$ with$[Cu^I_2(mphenpr)_2]^{2+}$ was investigated with helicate solutions containing $\sim$ 0.01 M CCl_4 in CH_3OH where the spontaneous oxidation $[Cu^I_2(mphenpr)_2]^{2+}$ is very slow. Also the reaction of $C^{\bullet}Cl_3$ with $[Cu^I_2(mphenpr)_2]^{2+}$ can be observed in this medium condition without the interference from the species formed during the unfolding process, eqs 3, 4. Blank experiments were conducted so as to establish whether the reactions of $[Cu^I_2(mphenpr)_2]^{2+}$ with e^-_{sol} and $C^{\bullet}H_2OH$ radicals (produced by the radiolysis of CH_3OH, Scheme 1) interfere with the reaction of $C^{\bullet}Cl_3$ with $[Cu^I_2(mphenpr)_2]^{2+}$. Pulse radiolysis of 10^{-4} M $[Cu^I_2(mphenpr)_2]^{2+}$ in N_2-saturated CH_3OH, where e^-_{sol} and $C^{\bullet}H_2OH$ radicals were produced with large yields, caused changes in the absorption spectrum of the solution that are consistent with the reduction of a phenanthroline group to produce $[Cu^I_2(mphenpr)(mphenpr\bullet)]^+$, Figure 7. Conversely, no changes in the spectrum of $[Cu^I_2(mphenpr)_2]^{2+}$ were observed in the radiolysis of N_2O-saturated CH_3OH solutions where only $C^{\bullet}H_2OH$ radicals can react with the helicate. Therefore, it was concluded that e^-_{sol} reacts with $[Cu^I_2(mphenpr)_2]^{2+}$ to form $[Cu^I_2(mphenpr)(mphenpr^{\bullet})]^+$, eq 9.

$$[Cu^I_2(mphenpr)_2]^{2+} + e^-_{sol} \rightarrow [Cu^I_2(mphenpr)(mphenpr\bullet)]^+ \quad (9)$$

A rate constant, $k = 1.6 \times 10^8$ M^{-1} s^{-1}, was calculated for eq 9 from the time-resolved 600 nm absorbance growth and the bleach of the 445 nm absorbance. Considering the value of this rate constant and that of the rate constant for the reaction of e^-_{sol} with CCl_4, $k = 1.6 \times 10^{10}$

(62) Wenwort, W. E.; George, R.; Keith, H. *J. Chem. Phys.* **1969**, *51*, 1791–1798.
(63) Wenwort, W. E.; Becker, R. S.; Tung, R. *J. Phys. Chem.* **1967**, *71*, 1652–1658.
(64) Andrieux, C. P.; Le Gorande, A.; Savéant, J.-M. *J. Am. Chem. Soc.* **1992**, *114*, 6892–6904.
(65) Chateauneuf, J.; Lusztyk, J.; Ingold., K. *J. Org. Chem.* **1990**, *55*, 1061–1065.

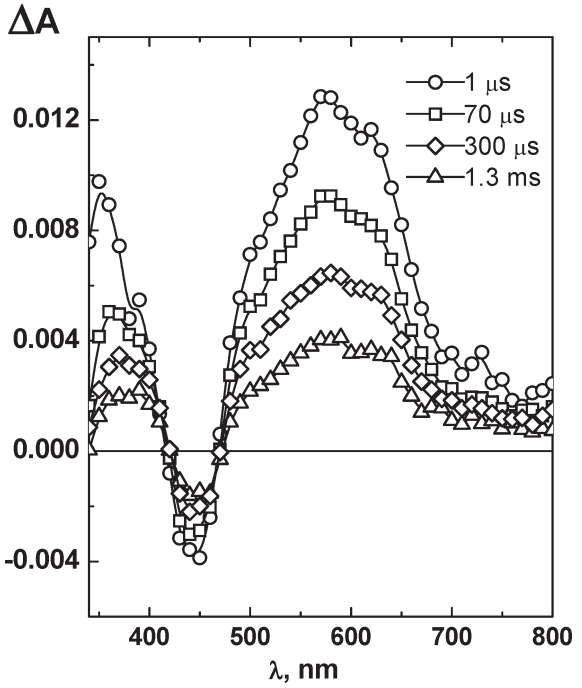

Figure 7. Decay of the difference spectrum of $[Cu^{I}_2(mphenpr)(mphenpr^{\bullet})]^{+}$. The coordinated ligand radical was generated in less than 1 μs by the reaction of e^{-}_{sol} with 1×10^{-4} M $[Cu^{I}_2(mphenpr)_2]^{2+}$ in N_2-saturated CH_3OH.

M^{-1} s^{-1},[66] it becomes evident that the e^{-}_{sol} reacts quantitatively with the CCl_4 to produce Cl^{-} and $C^{\bullet}Cl_3$ in a N_2-saturated solution containing 10^{-4} M helicate and 0.01 M CCl_4 in CH_3OH. After the generation of $C^{\bullet}Cl_3$, the reaction of the $C^{\bullet}Cl_3$ radicals with $[Cu^{I}_2(mphenpr)_2]^{2+}$ bleaches the MLCT band over a millisecond time scale. A very weak absorption band in the 550−600 nm region of the spectrum evolved simultaneously with the bleach of the MLCT band. Given that the absorption bands of $[Cu^{II}(mphenpr)]^{2+}$ are located in the 750−1000 nm range, Figure 5, the features at 550−600 nm were tentatively attributed to the formation of a precursor of the $[Cu^{II}(mphenpr)]^{2+}$ product. On the basis of literature reports that have communicated the formation of species with Cu−C bonds when C-centered radicals react with Cu(I) complexes,[67,68] the intermediate can most likely be represented as $[Cu^{I}Cu^{II}(CCl_3)(mphenpr)_2]^{2+}$, eqs 10, 11.

$$[Cu^{I}_2(mphenpr)_2]^{2+} + C\bullet Cl_3 \xrightarrow{k} [Cu^{I}Cu^{II}CCl_3(mphenpr)_2]^{2+} \quad (10)$$

$$[Cu^{I}Cu^{II}CCl_3(mphenpr)_2]^{2+} + H^{+}\cdots \rightarrow [Cu^{II}(mphenpr)^{2+} + CHCl_3 + [Cu^{I}(mphenpr)]^{+} \quad (11)$$

Absorbance traces recorded at 445 nm were fit to an exponential, $\Delta A = \Delta A_0 \exp(-k_{obs}\, t)$, with a pseudo-first order rate constant, $k_{obs} = 8.7 \times 10^4$ s^{-1}. A second order rate constant, $k = 9.1 \times 10^7$ s^{-1} M^{-1}, was calculated from the dependence of k_{obs} on $[Cu^{I}_2(mphenpr)_2]^{2+}$ concentration.

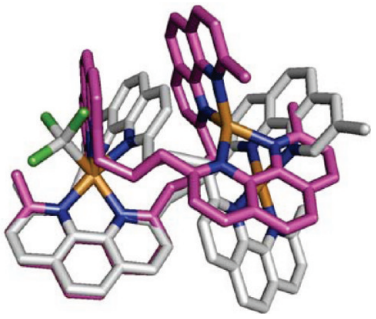

Figure 8. DFT optimized structures of the $[Cu^{I}Cu^{II}(CCl_3)(mphenpr)_2]^{2+}$ intermediate superimposed with the X-ray $[Cu^{I}_2(mphenpr)_2]^{2+}$ (purple). The helicate structure (purple) is included to help understand the distortion. H atoms are omitted for clarity.

Theoretical calculations were used to verify the thermochemical stability of the proposed $[Cu^{I}Cu^{II}(CCl_3)(mphenpr)_2]^{2+}$ intermediate. To this end, the coordination of the $C^{\bullet}Cl_3$ radical has been modeled, rendering a stable structure, Figure 8, where the local tetrahedral symmetry on the Cu center has changed to square pyramidal. The calculated UV−vis spectrum shows low intensity features with peaks at 575 and 640 nm associated with transitions from the ligands to a SOMO with electron density in the $C^{\bullet}Cl_3$ radical and the Cu atom bonded to it. These features agree with those observed in the spectrum of the $[Cu^{I}Cu^{II}(CCl_3)(mphenpr)_2]^{2+}$ produced in pulse radiolysis experiments, supporting the probable formation of the intermediate proposed in eq 10.

The generation of short-lived Cu^{II}-alkyl complexes when C-centered radicals react with Cu(I) complexes[67,69,70] suggested that the helicate should undergo similar reactions with radicals other than the $C^{\bullet}Cl_3$. To investigate if the formation of helicates with Cu−C bonds constitutes a common pathway, the reactions of other C-centered radicals with $[Cu^{I}_2(mphenpr)_2]^{2+}$ were also investigated by pulse radiolysis. The $C^{\bullet}HCl_2$ and $C^{\bullet}H_2Cl$ radicals were prepared by the reaction of e^{-}_{sol} with 1 M $CHCl_3$ and CH_2Cl_2 respectively in CH_3OH containing 10^{-4} M of the Cu(I) complex. No reaction between $[Cu^{I}_2(mphenpr)_2]^{2+}$ and $C^{\bullet}H_2Cl$ radicals was observed, and the reaction with $C^{\bullet}HCl_2$ radicals was an inefficient process producing barely discernible changes in the spectrum of the solution. An increasing electron affinity of the radicals with the number of chlorine atoms accounts for the observed reactivity. The reaction between $[Cu^{I}_2(mphenpr)_2]^{2+}$ and C-centered radicals is not limited to aliphatic radicals. Both $C_6H_5^{\bullet}$ and $C_{10}H_7^{\bullet}$ react with $[Cu^{I}_2(mphenpr)_2]^{2+}$ producing new absorption bands in the 500−600 nm region of the spectrum. These new absorption bands are located at longer wavelengths than the intense absorption bands of the $C_6H_5^{\bullet}$ and $C_{10}H_7^{\bullet}$ radicals placed at $\lambda < 450$ nm and must be

(66) Afanassiev, A. M.; Okazaki, K.; Freeman, G. R. *J. Phys. Chem.* **1979**, *83*, 1244–1249.
(67) Ferraudi, G. *Inorg. Chem.* **1978**, *17*, 2506–2508.
(68) Buxton, G. V.; Sellers, R. M. *Coord. Chem. Rev.* **1977**, *22*, 195–274.
(69) Navon, N.; Golub, G.; Cohen, H.; Meyerstein, D. *Organometallics* **1995**, *14*, 5670–5676.
(70) Masarwa, M.; Cohen, H.; Meyerstein, D. *Inorg. Chem.* **1986**, *25*, 4897–4900.

attributed to the formation of $[Cu^{I}Cu^{II}(R)(mphenpr)_2]^{2+}$ species where R = C_6H_5 and $C_{10}H_7$, eq 12.

$$[Cu^{I}2(mphenpr)_2]^{2+} + R^{\bullet} \rightarrow [Cu^{I}Cu^{II}(R)(mphenpr)_2]^{2+} \quad (12)$$

The kinetics of the reaction of $C_{10}H_7^{\bullet}$ radicals with $[Cu^{I}_2(mphenpr)_2]^{2+}$ was investigated as a function of the complex concentration. Deaerated methanolic solutions containing 5×10^{-2} M $C_{10}H_7Cl$ and the following concentrations of complex 1.0×10^{-3} M, 5.0×10^{-4} M, 1.0×10^{-4} M, or 6.3×10^{-5} M were used in these experiments. The parameter ξ was calculated from the absorbance change at 440 nm, and it was fitted to an exponential function, $\exp(-k_{obs}t)$, where k_{obs} is the rate constant of the reaction run under a pseudo-first order regime on radical concentration. A graph of k_{obs} versus $[Cu^{I}_2(mphenpr)_2]^{2+}$ concentration was linear with a slope, $k = 3.7 \times 10^6$ M^{-1} s^{-1}, corresponding to the rate constant of the reaction of the $C_{10}H_7^{\bullet}$ radicals with $[Cu^{I}_2(mphenpr)_2]^{2+}$, eq 12. The intercept, ${t_{1/2}}^{-1} = 1.1 \times 10^3$ s^{-1}, is in accordance with the expected half-life period, $t_{1/2}$, of the radical−radical annihilation reaction, eq 13, given the $C_{10}H_7^{\bullet}$ concentration, $\sim 3 \times 10^{-6}$ M, produced by the radiolytic pulse.

$$2C_{10}H_7^{\bullet} \rightarrow (C_{10}H_7)_2 \quad (13)$$

Concluding Remarks

The helical structure $[Cu^{I}_2(mphenpr)_2]^{2+}$ displays interesting properties in relation to both its associated mechanisms and its practical applications. Temperature and solvent affected the reversible equilibrium between $[Cu^{I}_2(mphenpr)_2]^{2+}$ and $[Cu^{I}(mphenpr)]^{+}$. Moreover, the kinetics of the $[Cu^{I}_2(mphenpr)_2]^{2+}$ unfolding is more complex than those observed with other helicates.[17,58,71,72] It is consistent with the formation of a binuclear reaction intermediate, $\{[Cu^{I}_2(mphenpr)_2]^{2+}\}^*$, with either a face-to-face configuration or a partially dissociated Cu(I) center. If $\{[Cu^{I}_2(mphenpr)_2]^{2+}\}^*$ is a binuclear complex with a face-to-face configuration, its lack of stability stands in contrast with other face-to-face isomers of structurally related helicates.[58,72] On the other hand, the mechanistic information on the substitution reactions of chelates[59] suggests that $\{[Cu^{I}_2(mphenpr)_2]^{2+}\}^*$ could be a species with a partially dissociated Cu(I) center. Irrelevant of the actual configuration of $\{[Cu^{I}_2(mphenpr)_2]^{2+}\}^*$, it appears that the thermochemical stability of the species follows the trend $[Cu^{I}_2(mphenpr)_2]^{2+} < \{[Cu^{I}_2(mphenpr)_2]^{2+}\}^* < [Cu^{I}(mphenpr)]^{+}$ at room temperature and the reverse one at high temprerature.

While the solvent undoubtedly plays a role in the kinetics of the helicate's unfolding, the formation of the intermediate $\{[Cu^{I}_2(mphenpr)_2]^{2+}\}^*$ is also assisted by structural factors controlling the flexibility of the mphenpr ligand. The coordination sphere created by the phenanthroline groups around each Cu^{I} is more rigid than those defined by bpy and/or Schiff base ligands. In addition, the propylene bridge between the phenanthroline groups allows for a less hindered rotation of the ligands around the $Cu^{I}-Cu^{I}$ axis.

The oxidation of the helicate by CCl_4 is coupled to the unfolding process. From the stability of the $[Cu^{I}_2(mphenpr)_2]^{2+}$, $\{[Cu^{I}_2(mphenpr)_2]^{2+}\}^*$, and $[Cu^{I}(mphenpr)]^{+}$ toward the oxidation by CH_2Cl_2 and $CHCl_3$, it was concluded that the ionization potential of these species is smaller than the bond dissociation energy of the corresponding C−Cl bonds. Also, the ionization potential of the Cu(I) centers in $[Cu^{I}_2(mphenpr)_2]^{2+}$ cannot dissociate the C−Cl bond of CCl_4. The dissociation of the C−Cl bond of CCl_4 and the ensuing generation of the $C^{\bullet}Cl_3$ radical is accelerated by species formed in the conversion of $[Cu^{I}_2(mphenpr)_2]^{2+}$ to $[Cu^{I}(mphenpr)]^{+}$. This observation suggests that changes in the geometry of the ligands around the metal center, from tetrahedral in the helicate to more flattened tetrahedral in the other species, have provided the additional energy for the redox process. Such an effect is associated with the change in molecular architecture which is triggered by the different coordination preferences of Cu(II) and Cu(I).[25,26] The redox system $[Cu^{II}(mphenpr)]^{2+}/[Cu^{I}_2(mphenpr)_2]^{2+}$ has two stable states with distinctly different properties that can be easily interconverted, and can be classified thence as a redox switch.[73] From the structural point of view, it resembles the Cu^{II}/Cu^{I} system with the N_4 ligand 5,5′,3″,5″-tetramethyl-2,2′:6′:2″:6″:2‴-quaterpyridine, described by Lehn and co-workers.[74] As other C-centered radicals, that is, $C^{\bullet}HCl_3$, $C^{\bullet}H_2Cl$, $C_6H_5^{\bullet}$, and $C_{10}H_7^{\bullet}$, react with the helicate, the formation of species with Cu−C bonds appears to be a rather common reaction. The formation of similar reaction intermediates in dehalogenations induced by other polynuclear Cu(I) complexes[75] remains to be established.

Coupling the redox reaction to CCl_4 and other alkyl and aryl halocarbons has practical interest, as they represent the most frequently found contaminants in the atmosphere, soil, and underground water.[76,77] The study of the associated kinetics can help to find new ways to degrade pollutants through the understanding of the mechanism involved in the dechlorination process.[77]

Acknowledgment. L.L. thanks the financial support to Conicyt and Fondecyt by the Doctoral and AT-24060122-2006 grants, and to the Fulbright Commission in Chile. L.L. also thanks C. Adura and to Dr. C. Aliaga for their assistance with the NMR and EPR experiments. Samples for synchrotron crystallographic analysis were submitted through the SCrALS (Service Crystallography at Advanced Light Source) program. Crystallographic data were collected at Beamline 11.3.1 at the Advanced Light Source (ALS), Lawrence Berkeley National Laboratory. The ALS is supported by the U.S. Dept. of Energy, Office of Energy Sciences, under

(71) Krämer, R.; Lehn, J.-M.; Marquis-Rigault, A. *Proc. Natl. Acad. Sci. U.S.A.* **1993**, *90*, 5394–5398.
(72) Fatin-Rouge, N.; Blanc, S.; Leize, E.; Van Dorsselaer, A.; Baret, P.; Pierre, J.-L.; Albrecht-Gary, A.-M. *Inorg. Chem.* **2000**, *39*, 5771–5778.
(73) Gisselbrecht, J.-P.; Gross, M.; Lehn, J.-M.; Sauvage, J. -P.; Ziessel, R.; Piccinni-Leopardi, C.; Arrieta, J. M.; Germain, G.; Van Meersche, M. *Nouv. J. Chim.* **1984**, *8*, 659–667.
(74) Boulas, P. L.; Gomez-Kaifer, M.; Echegoyen, L. *Angew. Chem.* **1998**, *110*, 226–247.
(75) Lucchese, B.; Humphreys, K. J.; Lee, D.-H.; Incarvito, C. D.; Sommer, R. D.; Rheingold, A. L.; Karlin, K. D. *Inorg. Chem.* **2004**, *43*, 5987–5998.
(76) Laine, D. F.; Cheng., I. F. *Microchem. J.* **2007**, *85*, 183–193.
(77) *Climate Change 2007: The Physical Science Basis, Summary for Policymakers WMO*; 2007; Scientific assessment of ozone depletion, Global ozone research, and monitoring project report.

contract DE-AC02-05CH11231. The computational studies reported here were done on the Abe cluster at the National Center for Supercomputing Applications through a Teragrid Research Allocation. Generous allocation of computing resources by the Center for Research Computing at the University of Notre Dame is also acknowledged. The pulse radiolysis work described herein was supported by the Office of Basic Energy Sciences of the U.S. Department of Energy. This is Contribution No. NDRL-4824 from the Notre Dame Radiation Laboratory.

Supporting Information Available: Figure S1 with the ^{1}H NMR spectrum of 1,3-bis(9-methyl-1,10-henantrolin-2-yl)propane, mphenpr, in CD_3Cl; Figure S2 showing interplanar distance and deviation from a parallel arrangement of the planes of two 9-methyl-1,10-phenanthrolin-2-yl (mphenoliyl); Figure S3, S4, containing ^{1}H NMR, NOE coupling, and NOESY structural and spectroscopic information of $(mphenpr)_2$ and $[Cu^I_2(mphenpr)_2]^{2+}$; Figure S5, NMR-based calculation of K_T; Figure S6 showing a cyclic voltammogram of a solution of 5×10^{-4} M $[Cu^I_2(mphenpr)_2]^{2+}$ in CH_3CN with 0.10 M tetraethyl ammonium perchlorate as supporting electrolyte; Figure S7, solvent-dependent rates of the $[Cu^I_2(mphenpr)_2]^{2+}$ unfolding in CH_3CN, CH_2Cl_2, and CH_3OH; Figure S8, calculated concentrations of the $[Cu^I_2(mphenpr)_2]^{2+}$ and $[Cu^I(mphenpr)]^+$ as a function of time and the initial concentration of helicate; Figure S9, absorbance change at $\lambda_{obs} = 435$ nm as a function of time and helicate concentration; Figure S10, oxidation of $[Cu^I_2(mphenpr)_2]^{2+}$ by CCl_4; CIF files with the structures of the $[Cu^I_2(mphenpr)_2](ClO_4)_2$ and $[Cu^{II}(mphenpr)Cl](ClO_4)$. This material is available free of charge via the Internet at http://pubs.acs.org.